Commun. Comput. Phys.
doi: 10.4208/cicp.210211.011111a

Vol. **12**, No. 4, pp. 1070-1095
October 2012

The Space-Time CE/SE Method for Solving Reduced Two-Fluid Flow Model

Shamsul Qamar[1,2,*], Munshoor Ahmed[1] and Ishtiaq Ali[1]

[1] *Department of Mathematics, COMSATS Institute of Information Technology, Park Road, Chak Shahzad Islamabad, Pakistan.*
[2] *Max Planck Institute for Dynamics of Complex Technical Systems, Sandtorstr. 1, 39106 Magdeburg, Germany.*

Received 21 February 2011; Accepted (in revised version) 1 November 2011

Communicated by Boo Cheong Khoo

Available online 28 March 2012

Abstract. The space-time conservation element and solution element (CE/SE) method is proposed for solving a conservative interface-capturing reduced model of compressible two-fluid flows. The flow equations are the bulk equations, combined with mass and energy equations for one of the two fluids. The latter equation contains a source term for accounting the energy exchange. The one and two-dimensional flow models are numerically investigated in this manuscript. The CE/SE method is capable to accurately capture the sharp propagating wavefronts of the fluids without excessive numerical diffusion or spurious oscillations. In contrast to the existing upwind finite volume schemes, the Riemann solver and reconstruction procedure are not the building block of the suggested method. The method differs from the previous techniques because of global and local flux conservation in a space-time domain without resorting to interpolation or extrapolation. In order to reveal the efficiency and performance of the approach, several numerical test cases are presented. For validation, the results of the current method are compared with other finite volume schemes.

AMS subject classifications: 76T99, 65Y99, 65M99, 35L45, 35L65, 35L67

Key words: Reduced model, space-time CE/SE method, central schemes, conservation laws, hyperbolic systems, shock solutions.

1 Introduction

The physics of single-phase flow is relatively simple compared to two-phase flow due to existing moving and deformable interface and its interactions with the phases. Two-

*Corresponding author. *Email addresses:* shamsul.qamar@comsats.edu.pk (S. Qamar), manshoor@comsats.edu.pk (M. Ahmed), ishtiaqali@comsats.edu.pk (I. Ali)

phase flows are encountered in various scientific and engineering fields related to environmental research, chemical engineering processes, nuclear energy and advanced heat transfer systems. The modeling and simulation of such flows is one of the most challenging problems in computational fluid dynamics. The coupling of interface is challenge in these flows, as the coupling mismatch may generate large errors in the simulation. Significant efforts have been made in recent years to develop accurate general two-phase formulations, mechanistic models for interfacial transfer and interfacial structures and computational methods to solve these models.

This work is concerned with the computation of two fluid flow model of Kreeft and Koren [17]. In one space dimension, the selected model is a new formulation of the original Kapila's five-equation model [15]. The first four equations of the current model are similar to the Kapila's five equation model. These four equations describe the conservative quantities: two for mass, one for bulk momentum and one for bulk energy. The fifth equation corresponds to the energy equation for one of the two fluids and substitutes the topological equation in the Kapila's five equation model. In the fifth equation, the source term on the right hand side is responsible for energy exchange between the two fluids due to mechanical and thermodynamic works. The advantages of current model are the representation of all equations in integral form and as a single system. The current and original models are similar in differential form [17].

Several other models exist in the literature for describing the physics of two phase flows. These models use separate pressures, velocities and densities for each fluid. A convection equation for the interface motion is normally coupled with the conservation laws of flow models. In the literature such models are known as seven-equation models and are considered to be the most complete models. One of such models for solid-gas two-phase flows was initially introduced by Baer and Nunziato [3] and was further investigated by Abgrall and Saurel [1, 29–31], among others.

Apart from being complete, the seven-equation model possesses physical and numerical complexities. As the general physics of the model is not needed in several cases, simpler and more compact models were introduced in the literature ranging from three to six equation models [2, 4, 9, 10, 31]. The current model is more interesting due to the presence of differential source term in the energy equation for one of the two fluids. The solution of this model needs no explicit algorithm for the interface motion and, hence, can be easily implemented in the existing flow solvers. Other interface-tracking models, such as the volume-of-fluid [13] and level-set [24, 32] methods, require explicit equations for the interface motion. In the literature, different numerical methods have been proposed for solving two-phase flow models [1, 11, 16, 17, 27, 29, 33, 36].

In this article, a CE/SE method of Chang [5] is implemented for solving the selected reduced model in one and two space dimensions. In the two-dimensional case, a variant CE/SE method of Zhang et al. [35] is applied on rectangular mesh elements. The method is not an incremental improvement of a previously existing computational fluid dynamic (CFD) methods and is substantially different from other well-established methods. This method has many non-traditional features, such as unified treatment of space and time,

the introduction of conservation elements (CEs) and solution elements (SEs) and a novel shock capturing strategy without using Riemann solvers. The numerous applications of CE/SE method in different areas reveal the method's generality, feasibility and effectiveness. These areas include problems related to unsteady flows [5–7], vortex dynamics in aeroacoustics [20], diffusion problems [8], viscous flows [21], supersonic jets [19], inviscid and axisymmetric flows [18], magnetohydrodynamics [28] and electrical engineering [34]. For validation, the numerical results of CE/SE method are compared with the second order central schemes [14, 26] and second order kinetic flux-vector splitting scheme [27].

The rest of article is organized as follows. Section 2 gives a brief description of the selected two-phase flow model in two space dimensions. The current CE/SE method in two-dimensions is reviewed in Section 3. In Section 4, the reduced one-dimensional formulations of CE/SE method are given for the reader's understanding. In Section 5, numerical test cases are carried out. Finally, Section 6 gives conclusions and remarks.

2 Two-dimensional two-fluid flow model

In this section, the two-dimensional two-fluid flow model of Kreeft and Koren [17] is presented. In the derivation of the model, it is assumed that both fluids are mass conservative and have same velocity and pressure on both sides the interface. The same pressure and velocity are the major assumptions of reduced two-fluid models. Further, viscosity and heat conduction are neglected. In two space dimensions, this model consist of six equations, the first five equations describe the conservative quantities: two for mass, two for bulk momentums in the x and y-directions and one for bulk energy. The sixth equation is the energy equation for one of the two fluids and it includes source term on the right hand side which gives the energy exchange between two fluids in the form of mechanical and thermodynamical works. The state vector $\mathbf{q}$ of primitive variables has the form $\mathbf{q}=(\rho,\mathbf{u},p,\alpha)^T$. Here, ρ is the bulk mixture density, $\mathbf{u}=(u,v,0)$ are the bulk velocities along each characteristic direction, p is the bulk pressure and α is the volume fraction of fluid 1. This means that a part α of a small volume dV is filled with fluid 1 and a part $(1-\alpha)$ with fluid 2.

For bulk quantities, such as mixture density ρ and mixture specific total energy E, we assume that α is a volume fraction of fluid 1 and $(1-\alpha)$ of fluid 2. Using these conventions, we can define

$$\rho=\alpha\rho_1+(1-\alpha)\rho_2, \qquad \rho E=\alpha\rho_1E_1+(1-\alpha)\rho_2E_2, \tag{2.1}$$

where ρ_1 and ρ_2 denote the densities of fluid 1 and fluid 2, respectively. The total specific energies of each fluid are given as

$$E_1=e_1+\frac{1}{2}\mathbf{u}^2, \qquad E_2=e_2+\frac{1}{2}\mathbf{u}^2, \tag{2.2}$$

where e_1 and e_2 denote the specific internal energies of fluid 1 and fluid 2, respectively. The specific internal energies e_1 and e_2 can be written as a function of their respective densities and pressure through equations of state

$$e_1 = e_1(\rho_1, p), \qquad e_2 = e_2(\rho_2, p). \tag{2.3}$$

In two space dimensions, the two-fluid flow model can be written as [17]

$$\mathbf{w}_t + \mathbf{f}(\mathbf{w})_x + \mathbf{g}(\mathbf{w})_y = \mathbf{s}, \tag{2.4}$$

where

$$\mathbf{w} = (\rho, \rho u, \rho v, \rho E, \rho_1 \alpha, \rho_1 E_1 \alpha)^T, \tag{2.5a}$$

$$\mathbf{f}(\mathbf{w}) = (\rho u, \rho u^2 + p, \rho uv, \rho uE + pu, \rho_1 u\alpha, \rho_1 E_1 u\alpha + pu\alpha)^T, \tag{2.5b}$$

$$\mathbf{g}(\mathbf{w}) = (\rho v, \rho vu, \rho v^2 + p, \rho vE + pv, \rho_1 v\alpha, \rho_1 E_1 v\alpha + pv\alpha)^T, \tag{2.5c}$$

$$\mathbf{s}(\mathbf{w}) = (0,0,0,0,0,s_6)^T. \tag{2.5d}$$

Here, $\mathbf{w}$ represents the vector of conservative variables, $\mathbf{f}$, $\mathbf{g}$ are vectors of fluxes in x and y directions, $\mathbf{s}$ is a vector of source terms with only last non-zero term. The term s_6 represents the total rate of energy exchange per unit volume between fluid 1 and fluid 2 and is equal to the sum of rates of mechanical ${s_6}^M$ and thermodynamic ${s_6}^T$ works [17], i.e., $s_6 = {s_6}^M + {s_6}^T$, with

$${s_6}^M = u(p\alpha)_x + v(p\alpha)_y - \beta u p_x - \beta v p_y, \tag{2.6a}$$

$${s_6}^T = p\alpha(1-\alpha)\frac{\tau_2 - \tau_1}{\tau}(u_x + v_y). \tag{2.6b}$$

The term $\beta = \rho_1\alpha/\rho$ represents the mass fraction of fluid 1, while the relations $\tau_1 = 1/\rho_1 c_1^2$ and $\tau_2 = 1/\rho_2 c_2^2$ denote the isentropic compressibilities of both fluids. Here, c_1 and c_2 represent the sound speeds of fluid 1 and fluid 2. The bulk isentropic compressibility is defined as

$$\tau = \alpha\tau_1 + (1-\alpha)\tau_2. \tag{2.7}$$

The energy equation are directional independent, therefore for one- and two-dimensional problems the procedures of calculating primitive variables are the same. In two space dimensions, the primitive variables can be retrieved in the following manner. Assume that the equations of state in Eq. (2.3) are the stiffened equations of state [23]

$$\rho_1 e_i = \frac{p + \Pi_i \gamma_i}{\gamma_i - 1}, \qquad i = 1,2, \tag{2.8}$$

where γ_i and Π_i are the material specific quantities. Therefore, the sound speeds in each fluid are given as

$$c_i = \sqrt{\frac{(p + \Pi_i)\gamma_i}{\rho_i}}, \qquad i = 1,2. \tag{2.9}$$

The expressions for the sound speeds are normally obtained from the second law of thermodynamics. Let $|\mathbf{u}|:=\sqrt{u^2+v^2}$, the total energies of fluids 1 and 2 are given as

$$\rho_1 E_1\alpha=\frac{p+\Pi_1\gamma_1}{\gamma_1-1}\alpha+\frac{1}{2}\rho_1\alpha|\mathbf{u}|^2, \tag{2.10a}$$

$$\rho_2 E_2(1-\alpha)=\frac{p+\Pi_2\gamma_2}{\gamma_2-1}(1-\alpha)+\frac{1}{2}(\rho-\rho_1\alpha)|\mathbf{u}|^2. \tag{2.10b}$$

Using Eqs. (2.4), (2.10a) and (2.10b), we obtain

$$\rho=w_1,\quad u=\frac{w_2}{w_1},\quad v=\frac{w_3}{w_1}, \tag{2.11a}$$

$$\alpha=\begin{cases}\frac{\beta_1}{\beta_1+\beta_2}, & \text{if } \Pi_1=0=\Pi_2,\\ \frac{\Pi_2\gamma_2-\Pi_1\gamma_1-\beta_1-\beta_2\pm\sqrt{(\Pi_2\gamma_2-\Pi_1\gamma_1-\beta_1-\beta_2)^2+4\beta_1(\Pi_2\gamma_2-\Pi_1\gamma_1)}}{2(\Pi_2\gamma_2-\Pi_1\gamma_1)}, & \text{otherwise,}\end{cases} \tag{2.11b}$$

$$p=\beta_1+\beta_2-\alpha\Pi_1\gamma_1-(1-\alpha)\Pi_2\gamma_2, \tag{2.11c}$$

where

$$\beta_1=(\gamma_1-1)\Big(w_6-\frac{w_5(w_2^2+w_3^2)}{2w_1^2}\Big), \tag{2.12a}$$

$$\beta_2=(\gamma_2-1)\Big(w_4-w_6-\frac{(w_1-w_5)(w_2^2+w_3^2)}{2w_1^2}\Big). \tag{2.12b}$$

In Eq. (2.11b) the positive sign is chosen for $(\Pi_2\gamma_2-\Pi_1\gamma_1)>0$ and negative otherwise. Because of Eq. (2.9)

$$\tau_1=\frac{1}{\rho_1 c_1^2}=\frac{1}{(p+\Pi_1)\gamma_1},\qquad \tau_2=\frac{1}{\rho_2 c_2^2}=\frac{1}{(p+\Pi_2)\gamma_2}. \tag{2.13}$$

Next, the two-dimensional CE/SE method is implemented to solve the given model. In this scheme the non-differential parts of the source terms in Eqs. (2.6a) and (2.6b) are considered as cell averages, while the approximation of differential parts are analogous to the fluxes approximation.

3 Derivation of (CE/SE) method

In this section, the modified two-dimensional CE/SE method of Zhang et al. [35] on regular rectangular grids is briefly reviewed. Let t, x and y be the coordinates of a three-dimensional Euclidean space and, for $m=1,2,\cdots,6$, $\mathbf{h}_m=(w_m,f_m,g_m,-s_m)$ be the current density vectors in E_3. By applying Gauss-divergence theorem in E_3-space, Eq. (2.4) was found to be the differential form of the following integral conservation law

$$\oint_{S(V)}\mathbf{h}_m\cdot d\mathbf{S}=0,\qquad m=1,2,\cdots,6, \tag{3.1}$$

where m indicates the number of equations and $S(V)$ is the boundary of an arbitrary space-time domain V in the E_3-space. Eq. (3.1) is enforced over a space-time domain, called conservation element (CE), that allows the discontinuities of flow variables. The actual numerical integration is carried out in a discrete manner using solution elements (SEs). In SEs, the flow variables are assumed to be smooth and, hence, can be approximated by a specific function.

3.1 The space-time geometry of the CE and SE

To proceed, the entire computational domain is divided into non-overlapping uniform convex quadrilateral cells as shown in Fig. 1. The centroid of each cell is marked by a circle symbol that also represents the grid point in the modified CE/SE method, for instance point Q in Fig. 1(b). The set of these points is denoted by Ω. At each grid point one CE and associated one SE are constructed.

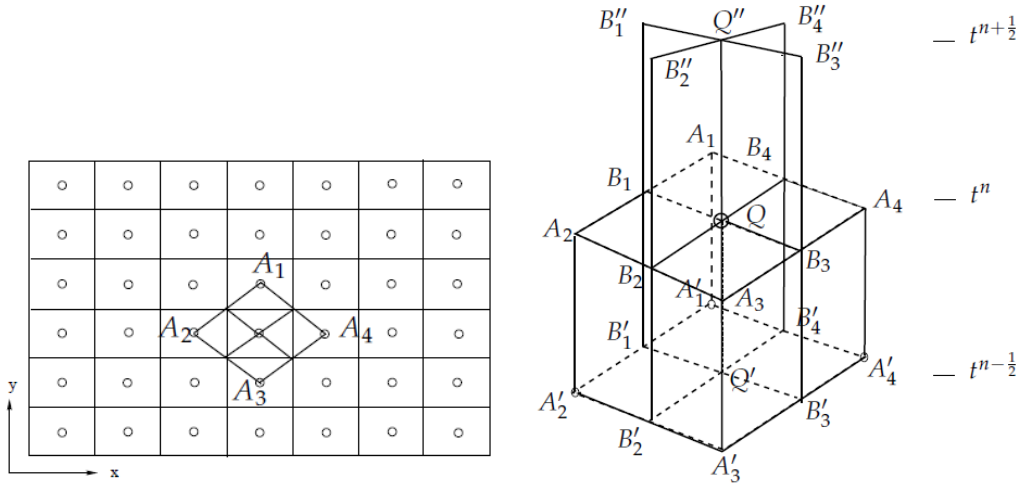

(a) (b)

Figure 1: Space-time geometry of the modified CE/SE method: (a) representative grid points in x-y plane, (b) the definitions of CE and SE.

In Fig. 1(b), the grid points Q, A_1, A_2, A_3 and A_4 are lying at time level $t=t^n$ at which the new numerical solutions of flow variables are to be calculated. The points Q', A_1', A_2', A_3' and A_4' are the corresponding points at time level $t=t^{n-1/2}$ and the points Q'', B_1'', B_2'', B_3'' and B_4'' are located at time level $t=t^{n+1/2}$. The same rule is applied to all mesh points for denoting the time levels. The SE associated to point Q is defined by the union of one horizontal plane segment $A_1A_2A_3A_4$ and two vertical plane segments $B_1''B_1'B_3'B_3''$ and $B_2''B_2'B_4'B_4''$. The CE associated to point Q is given by the cylinder $A_1B_1A_2B_2A_3B_3A_4B_4$ $A_1'B_1'A_2'B_2'A_3'B_3'A_4'B_4'$. The centroid Q of the top surface of this CE, denoted by polygon $A_1B_1A_2B_2A_3B_3A_4B_4$, is taken as the solution point. All the variables and their spatial derivatives are stored at point Q denoting the set of solution points Ω.

For $m=1,2,\cdots,6$, the distribution of w_m, f_m, g_m and s_m within SE are assumed to be continuous and can be approximated by first-order Taylor expansions about point Q. In other words, for any $(t,x,y)\in \mathrm{SE}(Q)$, $w_m(t,x,y)$ is approximated as

$$w_m^*(t,x,y)=(w_{mt})(t-t^n)+(w_m)_Q+(w_{mx})_Q(x-x_Q)+(w_{my})_Q(y-y_Q). \tag{3.2}$$

Similarly, one can write expressions for $f_m^*(t,x,y)$, $g_m^*(t,x,y)$ and $s_m^*(t,x,y)$. Here t^n, x_Q, y_Q, are the space-time coordinates of Q. The variables w_m,w_{mt}, w_{mx} and w_{my} on the left hand side of Eq. (3.2) are the discretized variables. If these variables are available, the flow solution structure within SE is fully specified. However, the above variables are not completely independent. Firstly, by employing Eq. (2.4), we obtain

$$(w_{mt})_Q=-(f_{mx})_Q-(g_{my})_Q+(s_m)_Q. \tag{3.3}$$

Secondly, chain rule can be used to calculate the $x-$derivatives of fluxes as

$$(f_{mx})_Q=(A_{mn})_Q(w_{nx})_Q,\qquad (g_{my})_Q=(B_{mn})_Q(w_{ny})_Q,\qquad m,n=1,\cdots,6, \tag{3.4}$$

where $(A_{mn})_Q$ and $(B_{mn})_Q$ denote the elements of the Jacobian matrices of f_m and g_m at point Q as given in Appendix. Analogously, other quantities can be calculated. Thus, $(w_m)_Q$, $(w_{mx})_Q$ and $(w_{my})_Q$ are the only independent discrete variables in each SE. After knowing these variables, the flow solution structure inside the SE is completely determined.

3.2 The calculation of flow variables W_m

To derive the scheme, the continuous space-time flux vector $\mathbf{h}_m(t,x,y)$ is replaced by a discrete one

$$\mathbf{h}_m^*(t,x,y)=(w_m^*(t,x,y),f_m^*(t,x,y),g_m^*(t,x,y),-s_m^*(t,x,y)) \tag{3.5}$$

and the Eq. (3.1) by its discrete counterpart

$$\oint_{S(CE(Q))}\mathbf{h}_m^*\cdot d\mathbf{S}=0. \tag{3.6}$$

On substituting Eqs. (3.2)-(3.5) into Eq. (3.6), the following algebraic equation can be obtained

$$(w_m)_Q^n=\frac{\left(\sum_{l=1}^4 R_m^{(l)}\right)}{S}, \tag{3.7}$$

where

$$\begin{aligned}R_m^{(l)}=&S_q^{(l)}\left[(w_m)_{A_l}^{n-1/2}+(x_q^{(l)}-x_{A_l})(w_{mx})_{A_l}^{n-1/2}+(y_q^{(l)}-y_{A_l})(w_{my})_{A_l}^{n-1/2}\right]\\&-\sum_{k=1}^{2}n_{kx}^{(l)}\left[(f_m)_{A_l}^{n-1/2}+(x_k^{(l)}-x_{A_l})(f_{mx})_{A_l}^{n-1/2}+\frac{\Delta t}{4}(f_{mt})_{A_l}^{n-1/2}\right]\end{aligned}$$

$$
\begin{aligned}
&-\sum_{k=1}^{2} n_{ky}^{(l)}\Big[(g_m)_{A_l}^{n-1/2}+(y_k^{(l)}-y_{A_l})(g_{my})_{A_l}^{n-1/2}+\frac{\Delta t}{4}(g_{mt})_{A_l}^{n-1/2}\Big]\\
&+\sum_{k=1}^{2} n_{kx}^{(l)}u_Q^{n-1/2}\Big[(s_m^1)_{A_l}^{n-1/2}+(x_k^{(l)}-x_{A_l})(s_{mx}^1)_{A_l}^{n-1/2}+\frac{\Delta t}{4}(s_{mt}^1)_{A_l}^{n-1/2}\Big]\\
&-\sum_{k=1}^{2} n_{kx}^{(l)}(\beta u)_Q^{n-1/2}\Big[(s_m^2)_{A_l}^{n-1/2}+(x_k^{(l)}-x_{A_l})(s_{mx}^2)_{A_l}^{n-1/2}+\frac{\Delta t}{4}(s_{mt}^2)_{A_l}^{n-1/2}\Big]\\
&+\sum_{k=1}^{2} n_{kx}^{(l)}(p\eta)_Q^{n-1/2}\Big[(s_m^3)_{A_l}^{n-1/2}+(x_k^{(l)}-x_{A_l})(s_{mx}^3)_{A_l}^{n-1/2}+\frac{\Delta t}{4}(s_{mt}^3)_{A_l}^{n-1/2}\Big]\\
&+\sum_{k=1}^{2} n_{ky}^{(l)}v_Q^{n-1/2}\Big[(s_m^1)_{A_l}^{n-1/2}+(y_k^{(l)}-y_{A_l})(s_{my}^1)_{A_l}^{n-1/2}+\frac{\Delta t}{4}(s_{mt}^1)_{A_l}^{n-1/2}\Big]\\
&-\sum_{k=1}^{2} n_{kx}^{(l)}(\beta v)_Q^{n-1/2}\Big[(s_m^2)_{A_l}^{n-1/2}+(y_k^{(l)}-y_{A_l})(s_{my}^2)_{A_l}^{n-1/2}+\frac{\Delta t}{4}(s_{mt}^2)_{A_l}^{n-1/2}\Big]\\
&+\sum_{k=1}^{2} n_{ky}^{(l)}(p\eta)_Q^{n-1/2}\Big[(s_m^4)_{A_l}^{n-1/2}+(y_k^{(l)}-y_{A_l})(s_{my}^4)_{A_l}^{n-1/2}+\frac{\Delta t}{4}(s_{mt}^4)_{A_l}^{n-1/2}\Big]. \qquad (3.8)
\end{aligned}
$$

According to Eqs. (2.6a) and (2.6b), we have

$$s_j^i=0, \quad \text{for } i=1,\cdots,4, \quad j=1,\cdots,5, \qquad (3.9a)$$

$$s_6^1=p\alpha, \quad s_6^2=p, \quad s_6^3=u, \quad s_6^4=v, \quad \eta=\alpha(1-\alpha)\frac{\tau_2-\tau_1}{\tau}. \qquad (3.9b)$$

It can be observed that the non-differential source terms in Eqs. (2.6a) and (2.6b) are taken as average values at point Q and the differential source terms are analogously approximated to the fluxes. Moreover, $l=1,2,3,4$ indicate the spatial flux contribution from the four neighbouring points and $m=1,2,\cdots,6$ are indicating the six flow equations. Here, Eq. (3.7) is used to calculate the numerical solution w_m at point Q. The geometrical treatments in Eqs. (3.7) and (3.8) are explained below (cf. Fig. 1). Let $l=1,2,3,4$ and $k=1,2$, then

1. The spatial coordinates of the four neighbouring solution points, i.e., points A_l, are denoted by (x_{A_l},y_{A_l}).
2. $(x_q^{(l)},y_q^{(l)})$ are the spatial coordinates of the centroids of four quadrilaterals $A_1B_1QB_4$, $A_2B_2QB_1$, $A_3B_3QB_2$ and $A_4B_4QB_3$.
3. $S_q^{(l)}$ are surface areas of the four quadrilaterals defined in 2.
4. $\mathbf{n}_k^{(l)}=(n_{kx}^{(l)},n_{ky}^{(l)},0)$, represent the eight surface vectors of the eight lateral planes: $A_1'B_4'A_1B_4$, $A_1'B_1'A_1B_1$, $A_2'B_1'A_2B_1$, $A_2'B_2'A_2B_2$, $A_3'B_2'A_3B_2$, $A_3'B_3'A_3B_3$, $A_4'B_3'A_4B_3$ and $A_4'B_4'A_4B_4$. Here, the surface vector is defined as the unit outward normal vector (outward from the interior of the CE) multiplied by its area.

5. $(t^{n-1/4}, x_k^{(l)}, y_k^{(l)})$ are the space-time coordinates of centroids of the eight lateral planes defined in 4.
6. S is the area of the polygon $A_1B_1A_2B_2A_3B_3A_4B_4$ that also represents the top surface of the present CE.

Note that, Eqs. (3.7) and (3.8) represent the space-time flux balance over the CE associated with point Q. The first term on the right hand side of Eq. (3.8) is the space-time flux through the bottom of the CE, contributed by the four neighboring cells at the time level $n-1/2$. The next four terms are the space-time fluxes through the eight lateral planes of the present CE. The remaining terms represent the approximation of source term. The fluxes and source terms on the right hand side of Eq. (3.8) are balanced by the space-time flux through the top surface of CE with area S. Due to linear distribution of flow variables, the flux through the top surface is simply given in term of w_m^n at central point Q multiplied by its area S. Because all flow conditions at the $n-1/2$ time level are known, Eqs. (3.7) and (3.8) represent an explicit method for calculating w_m^n at point Q.

3.3 Calculation of derivatives w_{mx} and w_{my} of flow variables

A central difference type reconstruction approach is employed to calculate $(w_{mx})_Q$ and $(w_{my})_Q$ [5,6,35]. Due to Taylor series

$$(w'_m)^n_{A_l} = (w_m)^{n-1/2}_{A_l} + \frac{\Delta t}{2}(w_{mt})^{n-1/2}_{A_l}, \qquad l = 1,2,3,4. \tag{3.10}$$

This predicted value actually represents a linear expansion in time. By using the values of $(w_m)^n_{A_1}$, $(w_m)^n_{A_2}$ and $(w_m)^n_Q$, the first pair of spatial derivatives of flow variables can be obtained, i.e., $w^{(1)}_{mx}$, $w^{(1)}_{my}$ at point Q:

$$w^{(1)}_{mx} = \frac{D_{mx}}{D}, \qquad w^{(1)}_{my} = \frac{D_{my}}{D}, \tag{3.11}$$

where

$$D = \begin{vmatrix} \Delta x_1 & \Delta y_1 \\ \Delta x_2 & \Delta y_2 \end{vmatrix}, \qquad D_{mx} = \begin{vmatrix} \Delta w^{(1)}_m & \Delta y_1 \\ \Delta w^{(2)}_m & \Delta y_2 \end{vmatrix}, \qquad D_{my} = \begin{vmatrix} \Delta x_1 & \Delta w^{(1)}_m \\ \Delta x_2 & \Delta w^{(2)}_m \end{vmatrix}, \tag{3.12a}$$

$$\Delta x_l = (x_{A_l} - x_Q), \qquad \Delta y_l = (y_{A_l} - y_Q), \qquad \Delta w^{(l)}_m = ((w'_m)^n_{A_l} - (w_m)^n_Q). \tag{3.12b}$$

Similarly, the solutions at A_2, A_3 and Q give the second pair $w^{(2)}_{mx}$ $w^{(2)}_{my}$, the solutions at A_3, A_4 and Q gives the third pair $w^{(3)}_{mx}$, $w^{(3)}_{my}$, while the solutions at A_1, A_4 and Q gives the fourth pair $w^{(4)}_{mx}$, $w^{(4)}_{my}$. Finally, a simple averaging gives w_{mx} and w_{my} at Q as follows:

$$(w_{mx})^n_Q = \frac{\left(\sum_{k=1}^4 w^{(k)}_{mx}\right)}{4}, \qquad (w_{my})^n_Q = \frac{\left(\sum_{k=1}^4 w^{(k)}_{my}\right)}{4}. \tag{3.13}$$

For flows with steep gradients or discontinuities, Eq. (3.13) is modified by a re-weighting procedure of the form [5, 6, 35]:

$$(w_{mx})_Q^n = \begin{cases} 0, & \text{if } \theta_{ml}=0,\ (l=1,2,3,4), \\ \sum_{k=1}^{4}[(w_m^{(k)})^\alpha w_{mx}^{(k)}] \Big/ \sum_{k=1}^{4}(w_m^{(k)})^\alpha, & \text{otherwise}, \end{cases} \tag{3.14a}$$

$$(w_{my})_Q^n = \begin{cases} 0, & \text{if } \theta_{ml}=0,\ (l=1,2,3,4), \\ \sum_{k=1}^{4}[(w_m^{(k)})^\alpha w_{my}^{(k)}] \Big/ \sum_{k=1}^{4}(w_m^{(k)})^\alpha, & \text{otherwise}, \end{cases} \tag{3.14b}$$

where

$$w_m^{(k)} = \prod_{l=1, l\neq k}^{4} \theta_{ml}, \qquad \theta_{ml} = \sqrt{(w_{mx}^{(l)})^2 + (w_{my}^{(l)})^2}. \tag{3.15}$$

In Eq. (3.14a), the value of adjustable constant α can be either 1 or 2. The Eqs. (3.14a) and (3.14b) are simple and effective to suppress spurious oscillations near the shocks. This concludes the formulation of two-dimensional CE/SE method on regular rectangular grids.

4 One-dimensional CE/SE method

For better understanding, it is advantageous to write down the reduced one-dimensional CE/SE method. It will help the reader in understanding the scheme.

In one space dimension, the two-fluid flow model (2.4) reduces to

$$\mathbf{w}_t + \mathbf{f}(\mathbf{w})_x = \mathbf{s}, \tag{4.1}$$

where

$$\mathbf{w} = \begin{pmatrix} \rho \\ \rho u \\ \rho E \\ \rho_1 \alpha \\ \rho_1 E_1 \alpha \end{pmatrix}, \qquad \mathbf{f}(\mathbf{w}) = \begin{pmatrix} \rho u \\ \rho u^2 + p \\ \rho u E + p u \\ \rho_1 u \alpha \\ \rho_1 E_1 u \alpha + p u \alpha \end{pmatrix}, \qquad \mathbf{s}(\mathbf{w}) = \begin{pmatrix} 0 \\ 0 \\ 0 \\ 0 \\ s_5 \end{pmatrix}. \tag{4.2}$$

Here, $s_5 = u(p\alpha)_x - \beta u p_x + p\alpha(1-\alpha)\frac{\tau_2-\tau_1}{\tau}u_x$. The scheme is based on the evolution of cell averages over staggered grids. The main marching scheme developed in [5] is given as

$$\mathbf{w}_{i+\frac{1}{2}}^{n+1/2} = \frac{1}{2}\left[\mathbf{w}_i^n + \mathbf{w}_{i+1}^n + \mathbf{z}_i^n - \mathbf{z}_{i+1}^n + \left(\mathbf{s}_{i+1}^{n+\frac{1}{4}} - \mathbf{s}_i^{n+\frac{1}{4}}\right)\right], \tag{4.3}$$

where

$$\mathbf{s}_{i+1}^{n+\frac{1}{4}} - \mathbf{s}_i^{n+\frac{1}{4}} = (0,0,0,0, {s_5}_{i+1}^{n+\frac{1}{4}} - {s_5}_i^{n+\frac{1}{4}})^T.$$

Moreover

$$\mathbf{z}_i^n = \frac{\Delta x}{4}(\mathbf{w}_x)_i^n + \frac{\Delta t}{\Delta x}\mathbf{f}_i^n + \frac{(\Delta t)^2}{4\Delta x}(\mathbf{f}_t)_i^n, \tag{4.4a}$$

$$\begin{aligned} {s5}_{i+1}^{n+\frac{1}{4}} - {s5}_i^{n+\frac{1}{4}} &= \frac{\Delta t}{2\Delta x}(u_i^{n+\frac{1}{4}} + u_{i+1}^{n+\frac{1}{4}})\left[(p\alpha)_{i+1}^{n+\frac{1}{4}} - (p\alpha)_i^{n+\frac{1}{4}}\right] \\ &\quad - \frac{\Delta t}{2\Delta x}\beta_i^{n+\frac{1}{4}}(u_i^{n+\frac{1}{4}} + u_{i+1}^{n+\frac{1}{4}})\left[p_{i+1}^{n+\frac{1}{4}} - p_i^{n+\frac{1}{4}}\right] \\ &\quad + \frac{\Delta t}{\Delta x}(p\eta)_i^{n+\frac{1}{4}}\left[u_{i+1}^{n+\frac{1}{4}} - u_i^{n+\frac{1}{4}}\right], \end{aligned} \tag{4.4b}$$

for $\eta = \alpha(1-\alpha)\frac{\tau_2-\tau_1}{\tau}$. Here

$$\psi_i^{n+\frac{1}{4}} = \psi_i^n + \frac{\Delta t}{4}(\psi_t)_i^n, \quad \text{for } \psi \in \{u, p\alpha, \beta, p, p\eta\}. \tag{4.5}$$

Eq. (4.5) represents approximations in the source term. The numerical oscillations near a discontinuity can be suppressed by using the following limiting formulations for conservative variables slopes

$$(w_{mx})_{i+\frac{1}{2}}^{n+\frac{1}{2}} = U_m\left((w_{mx_-})_{i+\frac{1}{2}}^{n+\frac{1}{2}}, (w_{mx_+})_{i+\frac{1}{2}}^{n+\frac{1}{2}}; \alpha\right), \qquad m = 1, \cdots, 5. \tag{4.6}$$

Here, $1 \le \alpha \le 2$, $\mathbf{w}_x = [w_{1x}, w_{2x}, w_{3x}, w_{4x}, w_{5x}]^T$ and

$$U_m(x_-, x_+; \alpha) = \frac{|x_+|^\alpha x_- + |x_-|^\alpha x_+}{|x_+|^\alpha + |x_-|^\alpha}. \tag{4.7}$$

Moreover

$$(\mathbf{w}_{x_+})_{i+\frac{1}{2}}^{n+\frac{1}{2}} = \frac{(\mathbf{w}')_{i+1}^{n+\frac{1}{2}} - \mathbf{w}_{i+\frac{1}{2}}^{n+\frac{1}{2}}}{\Delta x/2}, \qquad (\mathbf{w}_{x_-})_{i+\frac{1}{2}}^{n+\frac{1}{2}} = \frac{\mathbf{w}_{i+\frac{1}{2}}^{n+\frac{1}{2}} - (\mathbf{w}')_i^{n+\frac{1}{2}}}{\Delta x/2} \tag{4.8}$$

and

$$(\mathbf{w}')_i^{n+\frac{1}{2}} = \mathbf{w}_i^n + \frac{\Delta t}{2}(\mathbf{w}_t)_i^n. \tag{4.9}$$

5 Numerical test problems

In this section, seven numerical test problems are presented. For validation, the numerical results of CE/SE method are compared with the results of second order central schemes [14,26] and second order kinetic flux-vector splitting (KFVS) scheme [27]. Except the test Problems 5.4 and 5.5, in all other problems $\Pi_1 = 0 = \Pi_2$.

5.1 One-dimensional test problems

The one-dimensional CE/SE method is applied to reproduce the discontinuous profiles of the so-called shock-tube problems. Given are the unitary numerical one-dimensional pipe and two constant states (ρ,u,p) of fluids 1 and 2, initially separated by a diaphragm placed at point $x=x_0$ of the pipe. After removing the diaphragm, typical patterns can be observed in the subsequent evolution namely, shocks, contact discontinuities and rarefaction waves.

Problem 5.1. Two-fluid sod's shock-tube problem

This problem is similar to the single-phase Sod's problem. The ratios of density and pressure have larger values and the left and right gases have different ratios of specific heats. The gases, initially at rest, are separated by a thin membrane located at $x=0.5$. The gas on the left side of the membrane has high density and pressure as compared to that on the right. After removing the membrane, the gases evolves in time and generate different patterns. The initial data are given as

$$(\rho,u,p,\alpha)=(10,0,10,1), \qquad \text{if } x\leq 0.5, \tag{5.1a}$$

$$(\rho,u,p,\alpha)=(0.125,0,0.1,0), \qquad \text{if } x>0.5. \tag{5.1b}$$

Here, $\gamma_L=1.4$, $\gamma_R=1.6$, $\Pi_L=0=\Pi_R$, $\alpha=1$ in Eq. (4.6) and CFL=0.5. The numerical results at $t=0.15$ are shown in Fig. 2. The solution contains a left-moving rarefaction wave, the right-moving shock wave and the right-moving two-fluid interface. The solution of CE/SE method is compared with other schemes at 200 mesh cells. All schemes give the correct positions of discontinuities and no pressure oscillations are visible in the solutions. It can be seen that the current scheme resolve sharp discontinuities better than other schemes.

Problem 5.2. The initial data are given as

$$(\rho,u,p,\alpha)=(2.0,0,1000,1), \qquad \text{if } x\leq 0.5, \tag{5.2a}$$

$$(\rho,u,p,\alpha)=(1,0,0.01,0), \qquad \text{if } x>0.5. \tag{5.2b}$$

Here, $\gamma_L=1.4$ and $\gamma_R=1.2$, $\Pi_L=0=\Pi_R$, $\alpha=1$ in Eq. (4.6) and CFL=0.5. This is a very hard test problem for a numerical scheme. The solution contain a left moving rarefaction wave, a contact discontinuity and a right moving shock wave. The right moving shock hits the interface at $x=0.5$. The shock continues to move towards right and a rarefaction wave is created which is moving towards left. We choose 400 mesh cells and the final simulation time is taken as $t=0.012$. The numerical results are shown in Fig. 3. The figures show that all schemes give comparable results. However, CE/SE method gives better resolution of peaks and discontinuities.

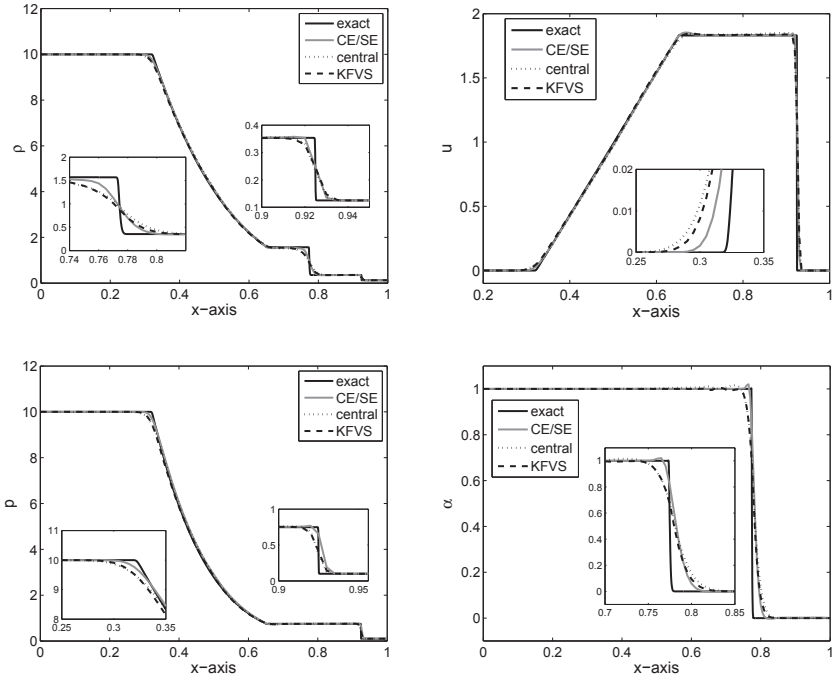

Figure 2: Results of Problem 5.1 on 200 mesh cells at $t=0.15$.

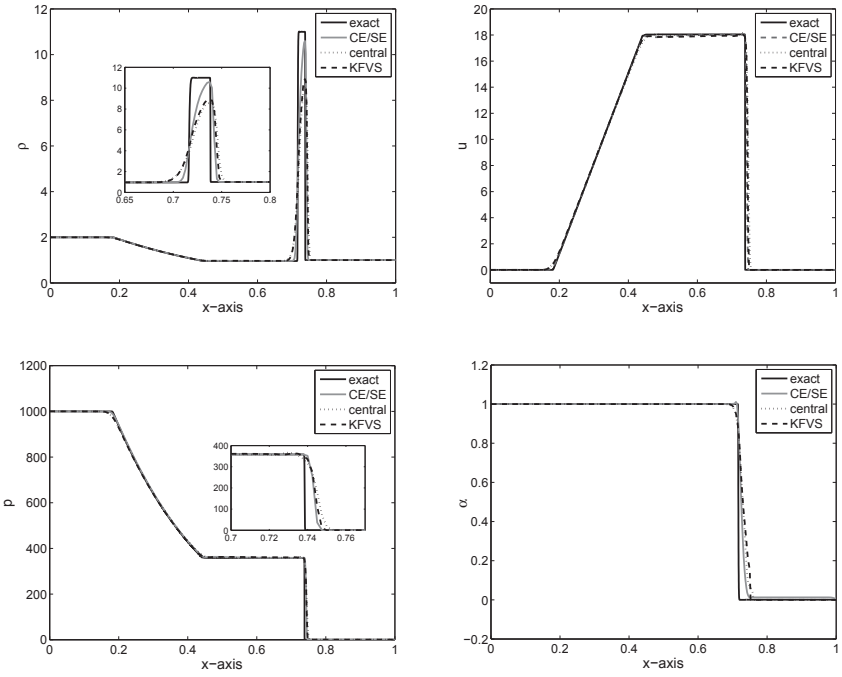

Figure 3: Results of Problem 5.2 on 400 mesh cells at $t=0.012$.

Problem 5.3. No-reflection problem

The initial data are given as

$$(\rho,u,p,\alpha)=(3.1748,9.435,100,1), \qquad \text{if } x\leq 0.5, \tag{5.3a}$$

$$(\rho,u,p,\alpha)=(1,0,1,0), \qquad \text{if } x>0.5. \tag{5.3b}$$

The ratio of specific heats are given as $\gamma_L=1.667$ and $\gamma_R=1.2$. Moreover, $\Pi_L=0=\Pi_R$, $\alpha=2$ in Eq. (4.6) and CFL=0.4. The domain $[0,1]$ is divided into 500 mesh cells and the final simulation time is $t=0.02$. This is also a hard test problem for a numerical scheme due to large jumps in pressure at the interface. The choice of pressure and velocity jump over the shock prevents the creation of a reflection wave, thus, only a shock wave moves to the right. The numerical results are shown in Fig. 4. The results of CE/SE method seems to be superior than other schemes. Moreover, wiggles are visible in the velocity and pressure plots of all schemes, representing small waves that are reflected to the left. However, unlike real velocity and pressure oscillations, these wiggles reduces on refined meshes. Similar wiggles can also be observed in the results of [17].

Problem 5.4. Water-air mixture problem

This one-dimensional problem corresponds to the water-air mixture problem [17,25]. The initial data are given as

$$(\rho,u,p,\alpha)=(525,0,10^9,0.5), \qquad \text{if } x\leq 0.5, \tag{5.4a}$$

$$(\rho,u,p,\alpha)=(525,0,10^5,0.5), \qquad \text{if } x>0.5. \tag{5.4b}$$

Here, $\gamma_L=1.4$, $\gamma_R=4.4$, $\Pi_L=0$, $\Pi_R=6\times10^8$, $\alpha=1$ in Eq. (4.6) and CFL=0.5. The domain $[0,1]$ is divided into 200 mesh cells and the final simulation time is $t=200\mu$s. The numerical results are shown in Fig. 5. Although the initial composition of the mixture is constant, it evolves in space and time. The results of CE/SE method are looking superior than other schemes. Moreover, our results are in good agreement with the simulations in [25] and thus verify that the present five equation model is a correct asymptotic limit of the seven equation model in the limit of zero relaxation time.

Problem 5.5. Water-air mixture problem

This one-dimensional problem corresponds to the water-air mixture problem [17,25]. This problem differs from the previous problem by allowing changes in the mixture composition. The initial data are given as

$$(\rho,u,p,\alpha)=(1,0,10^9,0.2), \qquad \text{if } x\leq 0.7, \tag{5.5a}$$

$$(\rho,u,p,\alpha)=(10^3,0,10^5,0.8), \qquad \text{if } x>0.7. \tag{5.5b}$$

Here, $\gamma_L=1.4$, $\gamma_R=4.4$, $\Pi_L=0$, $\Pi_R=6\times10^8$, $\alpha=1$ in Eq. (4.6) and CFL=0.5. The domain $[0,1]$ is divided into 200 mesh cells and the final simulation time is $t=200\mu$s. The numerical results are shown in Fig. 6. The results of CE/SE method are looking superior than other schemes. The numerical results are in good agreement with those published in [25].

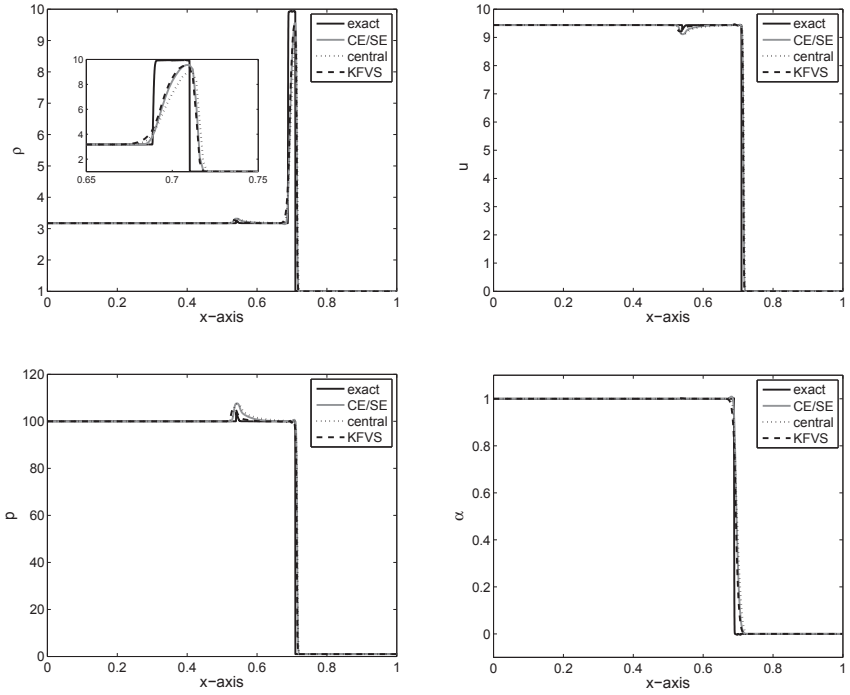

Figure 4: Results of Problem 5.3 on 500 mesh cells at $t=0.02$.

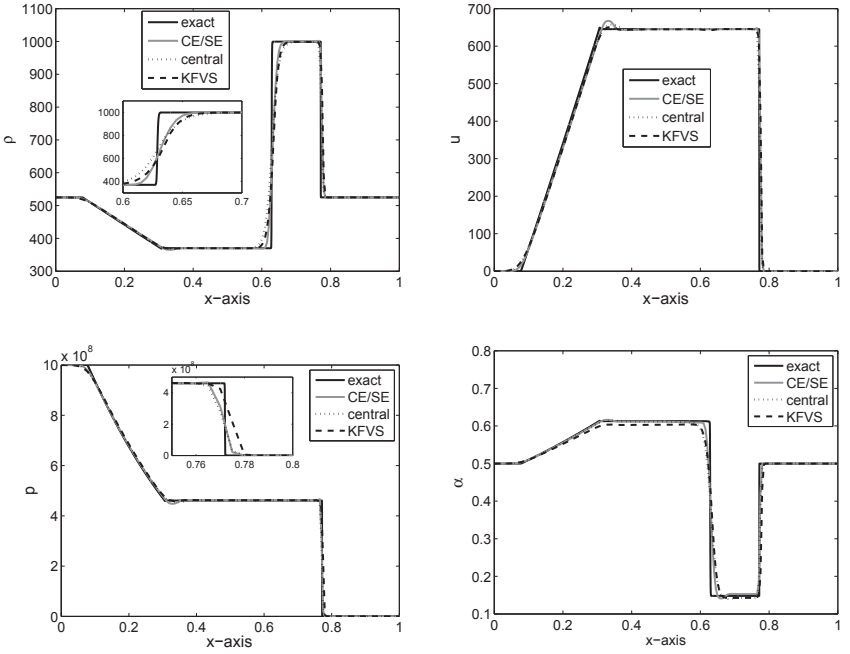

Figure 5: Results of Problem 5.4 on 200 mesh cells at $t=200\mu$s.

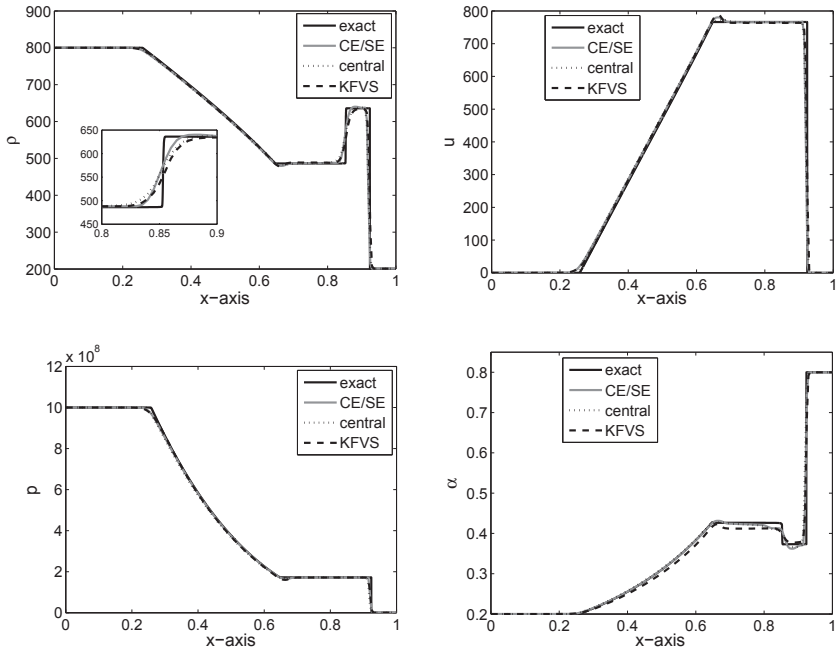

Figure 6: Results of Problem 5.5 on 200 mesh cells at $t=200\mu$s.

5.2 Two-dimensional test problems

The series of numerical experiments in one space dimension is ended by relevant test-problems in two space dimensions. Two test problems are considered for studying the impact of a shock in air on the bubbles of lighter and a heavier gases [12]. The numerical computations of these problems were reported, among others, by Quirk and Karni [16], Marquina and Mulet [22] and Kreeft and Koren [17]. A schematic computational setup is sketched in Fig. 7. A shock tube of length 4.5 and width 0.89 is considered. The tube has solid reflecting walls and open ends. Inside the tube a cylinder of very thin cellular walls is placed. The cylinder is filled with a gas and a left moving shock wave is generated at the right end of the tube. After hitting by shock, the walls of the cylinder ruptures and the shock starts interacting with the gas of the cylinder. Due to fast interaction both gases do not mix in large amount and, hence, generating a two-fluid flow problem. As the shock approaches to the surface of the bubble a reflected shock is generated from the surface of the bubble which moves towards right back in the air. At later time, this interaction become more and more complicated. The shock continues to move towards right in the air after passing through bubble and produces secondary reflected waves in the bubble when it hits the surface of the bubble.

The wave patterns generated by interaction are strongly depending on the density of the gas inside the bubble. However, some of these waves can be observed in all situations [17]. In this study, cylindrical bubbles of lighter helium and heavy R22 gases are considered.

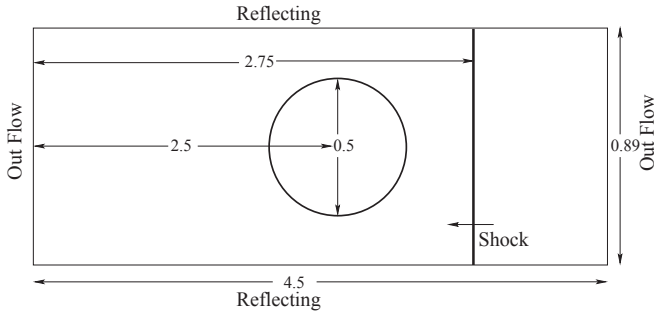

Figure 7: Sketch of computational domain.

Problem 5.6. Helium bubble

This problem corresponds to the interaction of $Ms=1.22$ planar shock, moving in air, with a cylindrical helium bubble contaminated with 28% of air. The bubble is assumed to be in thermodynamical and mechanical equilibrium with the surrounding air. The initial data are given as

$$\begin{aligned}
&(\rho,u,v,p,\gamma)=(1.4,0,0.0,1,1.4), && \text{pre-shock air},\\
&(\rho,u,v,p,\gamma)=(1.92691,-0.33361,0,1.5698,1.4), && \text{post-shock air},\\
&(\rho,u,v,p,\gamma)=(0.25463,0,0,1,1.648), && \text{helium}.
\end{aligned}$$

The position of key features occurred during the time evolution are well explained in [17, 22]. Therefore, we omit that discussion. Due to lower density and higher ratio of specific

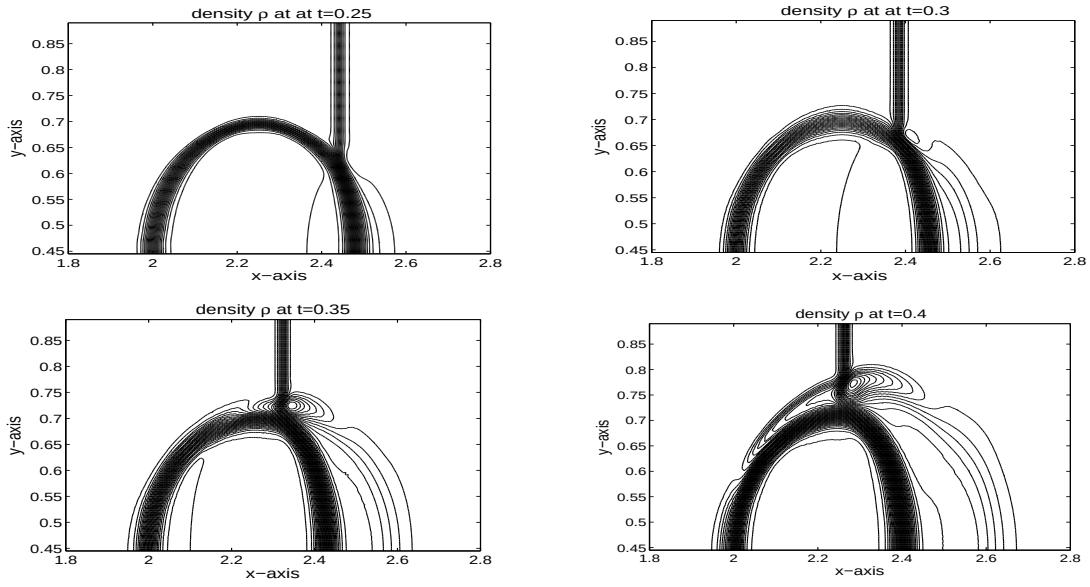

Figure 8: Density contours of Problem 5.6 (shock hitting helium bubble).

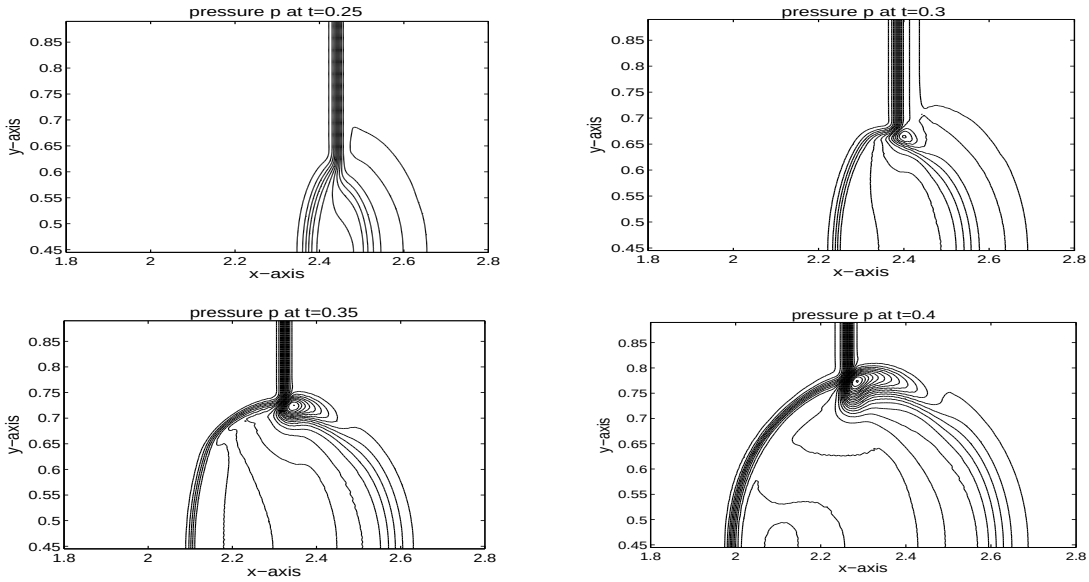

Figure 9: Pressure contours of Problem 5.6 (shock hitting helium bubble).

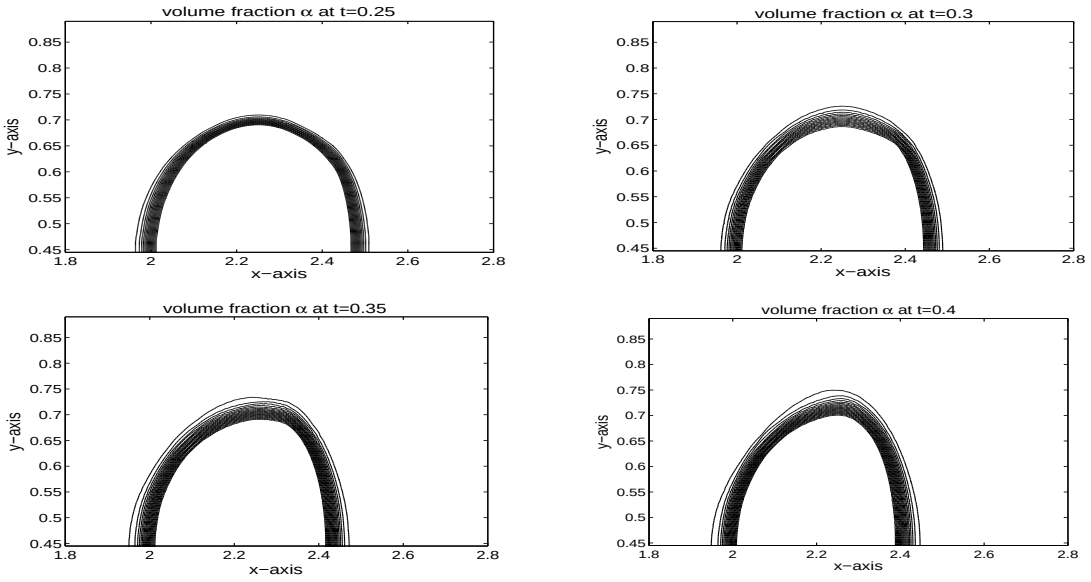

Figure 10: Volume fraction contours of Problem 5.6 (shock hitting helium bubble).

heats, the helium gas has larger speed of sound than air. As a result, the reflected shock runs ahead of the incoming shock and curving outwards. The computational domain is discretized into 800×200 mesh cells. Fig. 8 display the contours of density at times: 0.25, 0.3, 0.35 and 0.4. These results are closely matching with the plots given in [12, 16, 17]

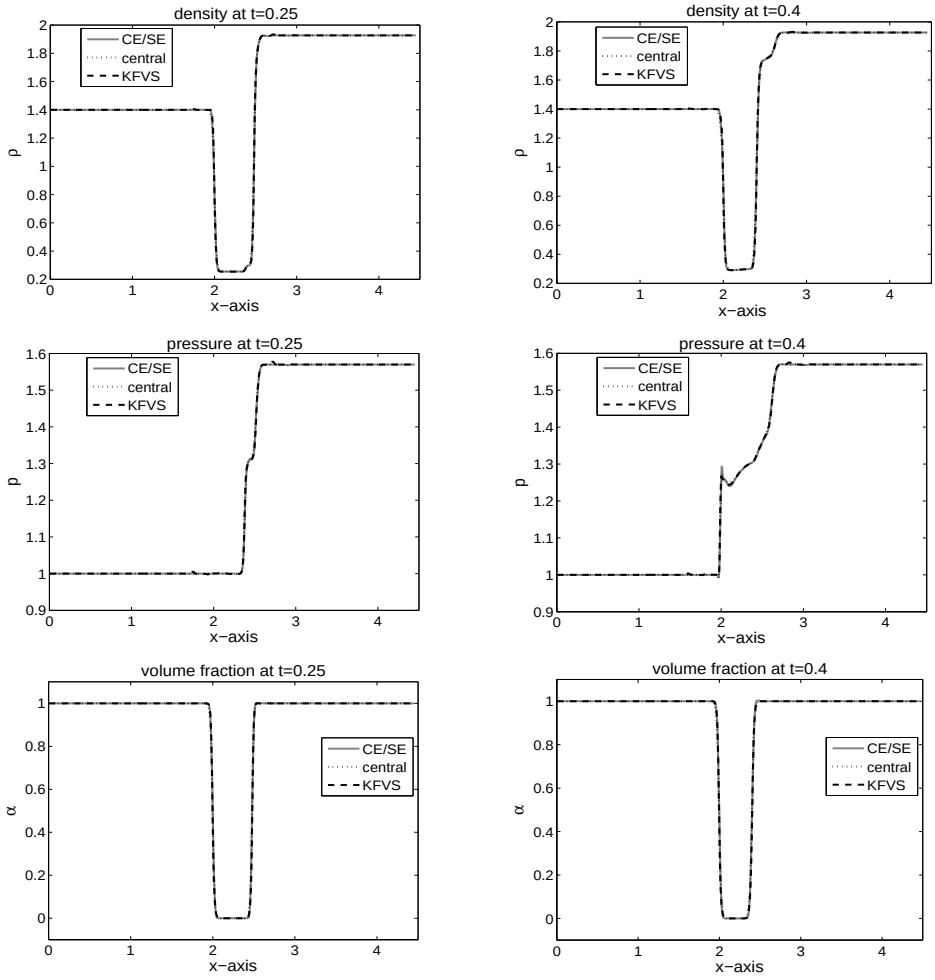

Figure 11: Plots along $y=0.445$ of Problem 5.6 (shock hitting helium bubble).

at times: 32μs, 52μs, 62μs, 82μs. The features used to match our contours with those in the literature are the relative position of some waves, such as refracted, transmitted or reflected shocks. Moreover, in Figs. 9 and 10 the contours of pressure and volume fraction show a perfect splitting of the pressure waves and the interface. The shocks and interface are sharp during the simulation. The last interface is slowly bending inwards in Fig. 10. The phenomena will continue at later times until the bubble split in two vortices. The one dimensional plots in Fig. 11, along the symmetry line $y=0.445$, compare the results of CE/SE, KFVS and central schemes. All schemes give comparable results.

Problem 5.7. R22 bubble

In this case the same $Ms=1.22$ planar shock hits a cylindrical R22 bubble which has higher density and lower ratio of specific heats than air. Thus, the lower speed of sound

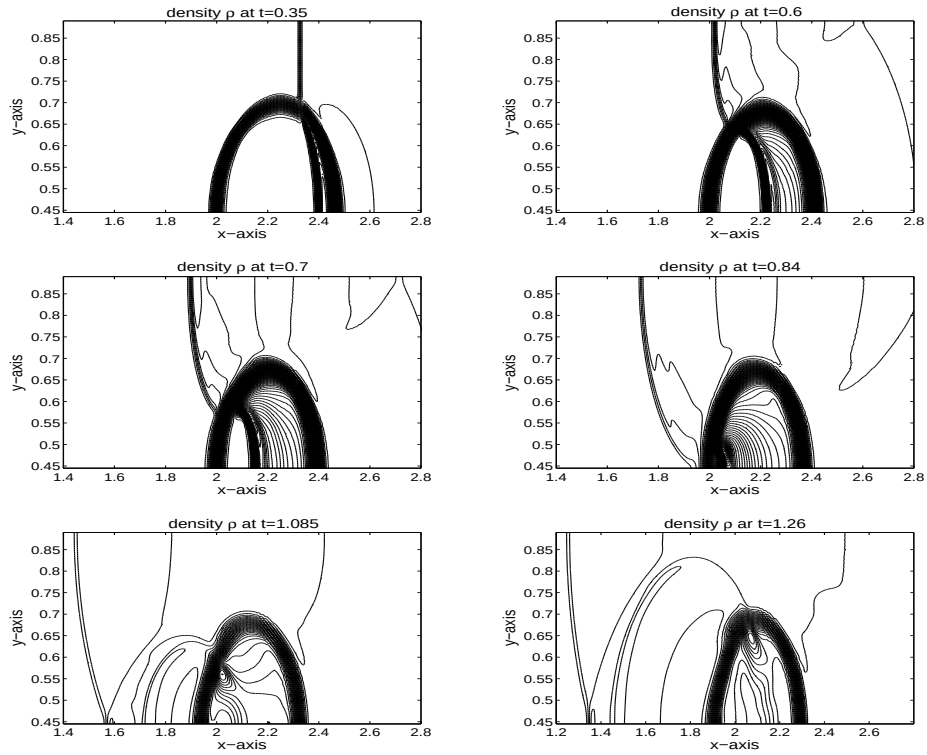

Figure 12: Density contours of Problem 5.7 (shock hitting R22 bubble).

is about two times lower than the previous case. The initial data are given as

$$(\rho,u,v,p,\gamma)=(1.40000,0.0,0.0,1.0,1.4), \qquad \text{pre-shock air},$$
$$(\rho,u,v,p,\gamma)=(1.92691,-0.33361,0.0,1.5698,1.4), \qquad \text{post-shock air},$$
$$(\rho,u,v,p,\gamma)=(4.41540,0.0,0.0,1.0,1.249), \qquad \text{R22}.$$

The computational domain is discretized into 800×200 mesh cells. Due to lower speed of sound, the shock in the bubble and the refracted shock lag behind the incoming shock. Further, because of circular bubble the refracted shock, the reflected wave and the shock wave are curved. The contours of density are shown in Fig. 12 at times: 0.35, 0.60, 0.70, 0.84, 1.085 and 1.26. These results are closely matching with the plots given in [12, 16, 17] at times: 55μs, 115μs, 135μs, 187μs, 247μs, 318μs. Moreover, in Figs. 13 and 14 contour plots of pressure and volume fraction are given. The flow pattern observed in the density contours is split well in a pressure and the interface. Moreover, no wiggles are visible in the results and the pressure is continuous over the interface. Hence, the numerical results of our scheme reflect all key features as explained in [12,17]. The one dimensional plots in Fig. 15, along the centerline $y=0.445$, compare the results of KFVS and central schemes. It is clear from the plots that both schemes have comparable accuracy.

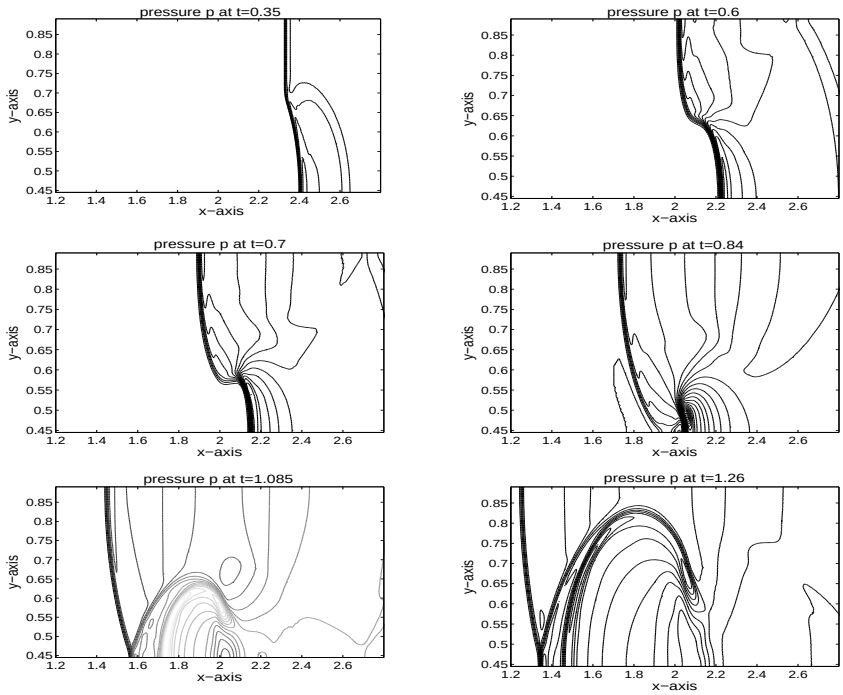

Figure 13: Pressure contours of Problem 5.7 (shock hitting R22 bubble).

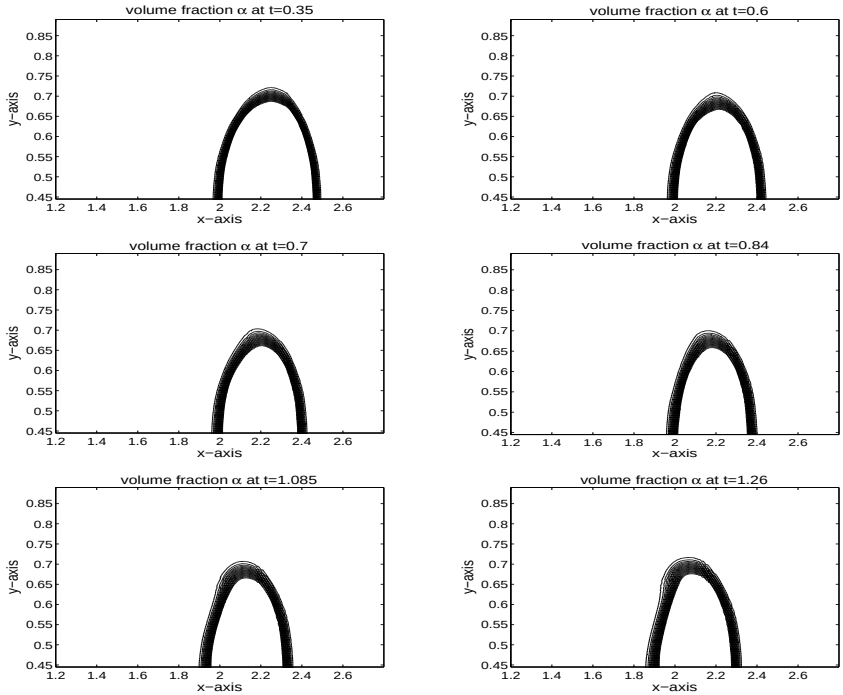

Figure 14: Volume fraction contours of Problem 5.7 (shock hitting R22 bubble).

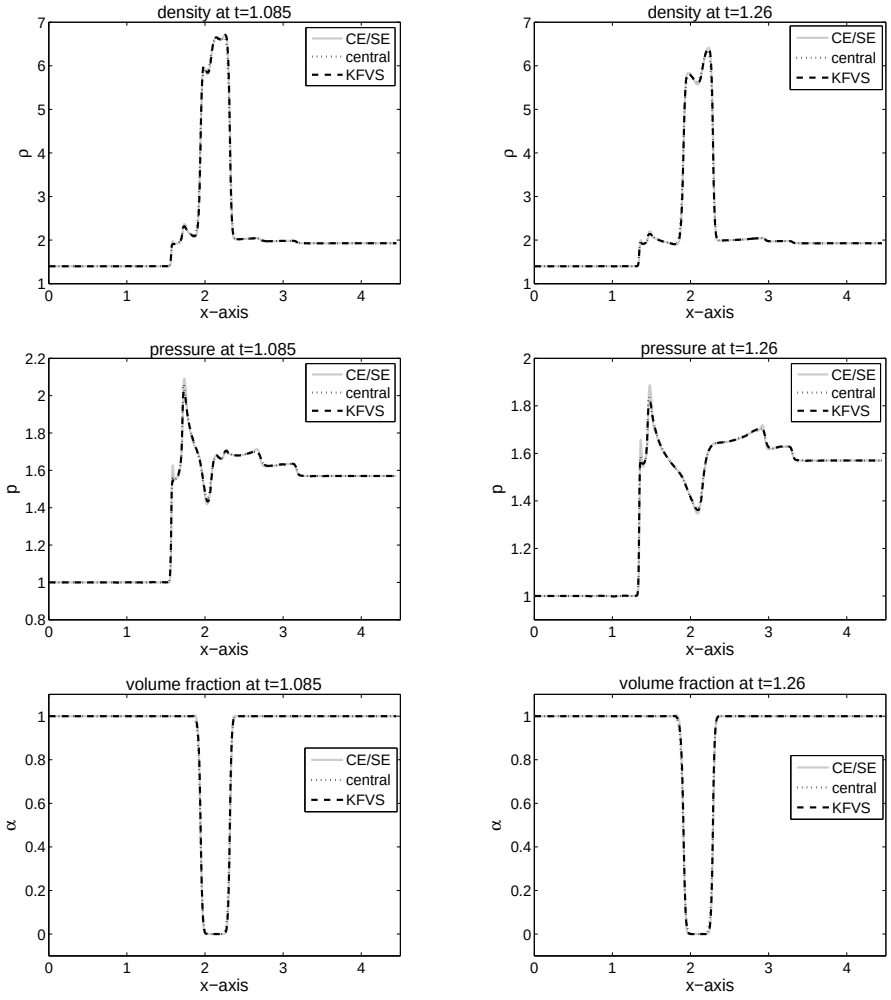

Figure 15: Plots along $y=0.445$ for Problem 5.7 (shock hitting R22 bubble).

6 Conclusions

The space-time CE/SE method was implemented for solving one and two dimensional compressible two-fluid models of Kreeft and Koren [17]. It was found that the method is capable to accurately captures the sharp propagating wavefronts of two-fluid flows without excessive numerical diffusion or spurious oscillations. The numerical results of the proposed method are in good agreement with those obtained from KFVS scheme, from central scheme and results available in the literature. It was found that CE/SE method gives better resolution of sharp peaks and discontinuities as compared to KFVS and central schemes. The current model is capable to accurately compute interface problems between compressible material and some two-phase flow problems where pressure and velocity equilibrium between the phases is reached. This work is a first step towards

the approximation of six and seven equations models by the same scheme. The seven-equation model is non-conservative and non-strictly hyperbolic, thus gives hard time to a numerical scheme. The present experience with the reduced model will help us to solve the six and seven equations models more efficiently and accurately.

Appendix: The Jacobian matrices in two-dimensional case

Let us define

$$\mathbf{u}^2=u^2+v^2,\quad M_1=\Big(\frac{1}{\gamma_1-1}-\frac{1}{\gamma_2-1}\Big)pu,$$

$$M_2=\Big(\frac{\alpha}{\gamma_1-1}-\frac{1-\alpha}{\gamma_2-1}\Big)p+\frac{1}{2}\rho(3u^2+v^2)+p,$$

$$M_3=\Big(\frac{\alpha}{\gamma_1-1}-\frac{1-\alpha}{\gamma_2-1}\Big)u+u,\quad \eta_1=\frac{w_2^2}{w_1^2}+\frac{w_3^2}{w_1^2},\quad \eta_2=1-\frac{w_5}{w_1},$$

$$p_{w_1}=(\gamma_1-1)\Big(\frac{w_5}{w_1}\eta_1\Big)+(\gamma_2-1)(\eta_1\eta_2-0.5\eta_2),$$

$$p_{w_2}=(\gamma_1-1)\Big(-\frac{w_5w_2}{w_1^2}\Big)-(\gamma_2-1)\Big((1-\eta_1)\frac{w_2}{w_1}\Big),$$

$$p_{w_3}=(\gamma_1-1)\Big(-\frac{w_5w_3}{w_1^2}\Big)-(\gamma_2-1)\Big((1-\eta_1)\frac{w_3}{w_1}\Big),$$

$$p_{w_5}=(\gamma_1-1)(-0.5\eta_1)+(\gamma_2-1)(0.5\eta_1),$$

$$\alpha_{w_1}=\frac{(\gamma_1-1)}{p}\Big(\frac{w_5}{w_1}\Big)\eta_1-\Big(\frac{\alpha}{p}\Big)p_{w_1},\quad \alpha_{w_2}=-\frac{(\gamma_1-1)}{p}\Big(\frac{w_5}{w_1}\Big)\Big(\frac{w_2}{w_1}\Big)-\Big(\frac{\alpha}{p}\Big)p_{w_2},$$

$$\alpha_{w_3}=-\frac{(\gamma_1-1)}{p}\Big(\frac{w_5}{w_1}\Big)\Big(\frac{w_3}{w_1}\Big)-\Big(\frac{\alpha}{p}\Big)p_{w_3},$$

$$\alpha_{w_5}=-\frac{(\gamma_1-1)}{2p}\eta_1-\Big(\frac{\alpha}{p}\Big)p_{w_5},\quad \alpha_{w_6}=\frac{(\gamma_1-1)}{p}-\Big(\frac{\alpha}{p}\Big)(\gamma_1-\gamma_2),$$

$$\zeta_1=u^2-2\rho u\frac{w_2}{w_1^2}+p_{w_1},\quad \zeta_2=uv-v\frac{w_2}{w_1}-u\frac{w_3}{w_1},$$

$$\theta_1=\frac{1}{2}\mathbf{u}^2u-M_2\Big(\frac{w_2}{w_1}\Big)-uv\Big(\frac{w_3}{w_1}\Big)+(M_3)(p_{w_1})+(M_1)(\alpha_{w_1}),$$

$$\theta_2=\frac{M_2}{w_1}+(M_3)(p_{w_2})+(M_1)(\alpha_{w_2}),\quad \theta_3=uv+(M_3)(p_{w_3})+(M_1)(\alpha_{w_3}),$$

$$\theta_4=(M_1+M_3)(\gamma_2-1),\quad \theta_5=(M_3)(p_{w_5})+(M_1)(\alpha_{w_5}),$$

$$\theta_6=(M3)(\gamma_1-\gamma_2)+(M_1)(\alpha_{w_6}),\quad M_4=\Big(\frac{\gamma_1}{\gamma_1-1}\Big)p\alpha+\frac{3}{2}\rho_1\alpha u^2+\frac{1}{2}\rho_1\alpha v^2,$$

$$\beta_1=-M_4\Big(\frac{w_2}{w_1^2}\Big)-(\rho_1\alpha uv)\Big(\frac{w_3}{w_1^2}\Big)+\Big(\frac{\gamma_1}{\gamma_1-1}\Big)(\alpha u(p_{w_1})+pu(\alpha_{w_1})),$$

$$\beta_2=\frac{M_4}{w_1}+\Big(\frac{\gamma_1}{\gamma_1-1}\Big)(\alpha u(p_{w_2})+pu(\alpha w_2)),$$

$$\beta_3=\frac{\rho_1\alpha uv}{w_1}+\Big(\frac{\gamma_1}{\gamma_1-1}\Big)(\alpha u(p_{w_3})+pu(\alpha w_3)),$$

$$\beta_4=\Big(\frac{\gamma_1}{\gamma_1-1}\Big)(\alpha u(p_{w_5})+pu(\alpha w_5))+\frac{1}{2}(u^3+uv^2),$$

$$\zeta_{12}=v^2-2\rho v\frac{w_3}{w_1^2}+p_{w_1},\quad N_1=\Big(\frac{1}{\gamma_1-1}-\frac{1}{\gamma_2-1}\Big)pv,$$

$$N_2=\Big(\frac{\alpha}{\gamma_1-1}-\frac{1-\alpha}{\gamma_2-1}\Big)v+v,\quad N_3=\Big(\frac{\alpha}{\gamma_1-1}-\frac{1-\alpha}{\gamma_2-1}\Big)p+\frac{1}{2}\rho(u^2+3v^2)+p,$$

$$N_4=\Big(\frac{\gamma_1}{\gamma_1-1}\Big)p\alpha+\frac{1}{2}\rho(u^2+3v^2),$$

$$\phi_1=\frac{1}{2}\mathbf{u}^2v-N_3\Big(\frac{w_3}{w_1}\Big)-uv\Big(\frac{w_2}{w_1}\Big)+(N_2)(p_{w_1})+(N_1)(\alpha_{w_1}),$$

$$\phi_2=uv+(N_2)(p_{w_2})+(N_1)(\alpha_{w_2}),\quad \phi_3=\frac{N_3}{w_1}+(N_2)(p_{w_3})+(N_1)(\alpha_{w_3}),$$

$$\phi_4=\Big(N_2-\frac{\alpha}{p}(N_1)\Big)(\gamma_2-1),\quad \phi_5=(N_2)(p_{w_5})+(N_1)(\alpha_{w_5}),$$

$$\phi_6=(N_2)(\gamma_1-\gamma_2)+(N_1)(\alpha_{w_6}),$$

$$\beta_5=\rho_1\alpha uv-N_4\Big(\frac{w_3}{w_1^2}\Big)+\Big(\frac{\gamma_1}{\gamma_1-1}\Big)(\alpha v(p_{w_1})+pv(\alpha w_1)),$$

$$\beta_6=\frac{\rho_1\alpha uv}{w_1}+\Big(\frac{\gamma_1}{\gamma_1-1}\Big)(\alpha v(p_{w_2})+pv(\alpha_{w_2})),$$

$$\beta_7=\frac{N_4}{w_1}+\Big(\frac{\gamma_1}{\gamma_1-1}\Big)(\alpha v(p_{w_3})+pv(\alpha_{w_3})),$$

$$\beta_8=\Big(\frac{\gamma_1}{\gamma_1-1}\Big)(\alpha v(p_{w_5})+pv(\alpha_{w_5}))+\frac{1}{2}(u^2+uv^3),$$

$$A_{mn}=\begin{pmatrix} u-\rho\dfrac{w_2}{w_1^2} & 1 & 0 & 0 & 0 & 0\\ \zeta_1 & 2u+p_{w_2} & p_{w_3} & \gamma_2-1 & p_{w_5} & \gamma_1-\gamma_2\\ \zeta_2 & v & u & 0 & 0 & 0\\ \theta_1 & \theta_2 & \theta_3 & \theta_4 & \theta_5 & \theta_6\\ -\rho_1\alpha\Big(\dfrac{w_2}{w_1^2}\Big) & \dfrac{\rho_1\alpha}{w_1} & 0 & 0 & 0 & 0\\ \beta_1 & \beta_2 & \beta_3 & 0 & \beta_4 & \gamma_1u \end{pmatrix},$$

$$B_{mn}=\begin{pmatrix} v-\rho\dfrac{w_3}{w_1^2} & 0 & 1 & 0 & 0 & 0\\ \zeta_2 & v & u & 0 & 0 & 0\\ \zeta_{12} & p_{w_2} & 2v+p_{w_3} & \gamma_2-1 & p_{w_5} & \gamma_1-\gamma_2\\ \phi_1 & \phi_2 & \phi_3 & \phi_4 & \phi_5 & \phi_6\\ -\rho_1\alpha\Big(\dfrac{w_3}{w_1^2}\Big) & 0 & \dfrac{\rho_1\alpha}{w_1} & 0 & v & 0\\ \beta_5 & \beta_6 & \beta_7 & 0 & \beta_8 & \gamma_1v \end{pmatrix}.$$

Acknowledgments

This work was partially supported by Higher Education Commission (HEC) of Pakistan through grant No. 1375.

References

[1] R. Abgrall and R. Saurel, Discrete equations for physical and numerical compressible multiphase mixtures, J. Comput. Phys., 186 (2003), 361–396.
[2] G. Allaire, S. Clerc and S. Kokh, A five-equation model for the simulation of interfaces between compressible fluids, J. Comput. Phys., 181 (2002), 577–616.
[3] M. R. Baer and J. W. Nunziato, A two-phase mixture theory for the deflagration-to-detonation transition in reactive granular materials, Int. J. Multiphase Flows, 12 (1986), 861–889.
[4] E. H. van Brummelen and B. Koren, A pressure-invariant conservative Godunov-type method for barotropic two-fluid flows, J. Comput. Phys., 185 (2003), 289–308.
[5] S. C. Chang, The method of space time conservation element and solution element-a new approach for solving the Navier-Stokes and Euler equations, J. Comput. Phys., 119 (1995), 295–324.
[6] S. C. Chang, X. Y. Wang and C. Y. Chow, New Developments in the Method of Space-Time Conservation Element and Solution Element-Applications to Two-Dimensional Time-Marching Problems, NASA TM 106758, 1994.
[7] S. C. Chang, X. Y. Wang and C. Y. Chow, The space-time conservation element and solution element method: a new high resolution and genuinely multidimensional paradigm for solving conservation laws, J. Comput. Phys., 156 (1999), 89–136.
[8] S. C. Chang, X. Y. Wang and W. M. To, Application of the space-time conservation element and solution element method to one-dimensional convection-diffusion problems, J. Comput. Phys., 165 (2000), 189–215.
[9] S. Clerc, Numerical simulation of the homogeneous equilibrium model for two-phase flows, J. Comput. Phys., 161 (2000), 354–375.
[10] H. Guillard and M. Labois, Numerical Modeling of Compressible Two-Phase Flows, in: P. Wesseling, E. Oñate, J. Périaux (Eds.), ECCOMAS CFD, 2006.
[11] J. -M. Ghidaglia, A. Kumbaro and G. L. Coq, On the numerical solution to two fluid models via a cell centered finite volume method, Euro. J. Mech. B Fluids, 20 (2001), 841–867.
[12] J. -F. Haas and B. Sturtevant, Interaction of weak shock waves with cylinderical and spherical gas inhomogeneities, J. Fluid Mech., 181 (1987), 41–76.
[13] C. W. Hirt and B. D. Nichols, Volume of fluid (VOF) method for the dynamics of free boundaries, J. Comput. Phys., 39 (1981), 201–225.
[14] G. -S. Jaing and E. Tadmor, Non-oscillatory central schemes for multidimensional hyperbolic conservation laws, SIAM J. Sci. Comput., 19 (1998), 1892–1917.
[15] A. K. Kapila, R. Menikoff, J. B. Bdzil, S. F. Son and D. S. Stewart, Two-phase modeling of deflagration-to-detonation transition in granular materials: reduced equations, Phys. Fluids, 13 (2001), 3002–3024.
[16] S. Karni1, E. Kirr, A. Kurganov and G. Petrova, Compressible two-phase flows by central and upwind schemes, ESAIM: M2AN, 38 (2004), 477–493.

[17] J. J. Kreeft and B. Koren, A new formulation of Kapila's five-equation model for compressible two-fluid flow and its numerical treatment, J. Comput. Phys., 229 (2010), 6220–6242.
[18] C. Y. Loh, L. S. Hultgren, S. C. Chang and P. C. E. Jorgenson, Noise Computation of a Shock-Containing Supersonic Axisymmetric Jet by the CE/SE Method, AIAA Paper 2000-0475, presented at the 38th AIAA Aerospace Sciences Meeting, January 10-13, Reno, NV, 2000.
[19] C. Y. Loh, L. S. Hultgren and S. C. Chang, Wave computation in compressible flow using the space-time conservation element and solution element method, AIAA J., 39 (2001), 794–801.
[20] M. Liu, J. B. Wang and K. -Q. Wu, The direct aero-acoustics simulation of flow around a square cylinder using the CE/SE scheme, J. Alg. Comput. Tech., 1 (2007), 525–537.
[21] C. Y. Loh and K. B. M. Q. Zaman, Numerical investigation of transonic resonance with a convergent-divergent nozzle, AIAA J., 40 (2002), 2393–2401.
[22] A. Marquina and P. Mulet, A flux-split algorithm applied to conservative model for multi-component compressible flows, J. Comput. Phys., 185 (2003), 120–138.
[23] R. Menikoff and B. J. Plohr, The Riemann problem for fluid flow of real materials, Rev. Mod. Phys., 61 (1989), 75–130.
[24] W. Mulder, S. Osher and J. A. Sethian, Computing interface motion in compressible gas dynamics, J. Comput. Phys., 100 (1992), 209–228.
[25] A. Murrone and H. Guillard, A five equation reduced model for compressible two phase flow problems, J. Comput. Phys., 202 (2005), 664–698.
[26] H. Nessyahu and E. Tadmor, Non-oscillatory central differencing for hyperbolic conservation laws, J. Comput. Phys., 87 (1990), 408–463.
[27] S. Qamar and M. Ahmed, A high order kinetic flux-vector splitting method for the reduced five-equation model of compressible two-fluid flows, J. Comput. Phys., 228 (2009), 9059–9078.
[28] S. Qamar and S. Mudasser, On the application of a variant CE/SE method for solving two-dimensional ideal MHD equations, Appl. Numer. Math., 60 (2010), 587–606.
[29] R. Saurel and R. Abgrall, A multiphase Godunov method for compressible multifluids and multiphase flows, J. Comput. Phys., 150 (1999), 425–467.
[30] R. Saurel, E. Franquet, E. Daniel and O. L. Metayer, A relaxation-projection method for compressible flows-part I: the numerical equation of state for the Euler equations, J. Comput. Phys., 223 (2007), 822–845.
[31] R. Saurel, F. Petitpas and R. A. Berry, Simple and efficient relaxation methods for interfaces separating compressible fluids, cavitating flows and shocks in multiphase mixtures, J. Comput. Phys., 228 (2009), 1678–1712.
[32] M. Sussman, P. Smereka and S. Osher, A level set approach for computing solutions to incompressible two-phase flow, J. Comput. Phys., 114 (1994), 146–159.
[33] E. Romenski, A. D. Resnyansky and E. F. Toro, Conservative hyperbolic formulation for compressible two-phase flow with different phase pressures and temperatures, Quart. Appl. Math., 65 (2007), 259–279.
[34] X. Y. Wang, C. L. Chen and Y. Liu, The space-time CE/SE method for solving Maxwell's equations in time domain, Antennas and Propagation Society International Symposium, IEEE 02/2002, 1 (2002), 164–167.
[35] Z. C. Zhang, S. T. Yu and S. C. Chang, A space-tome conservation element and solution element method for solving the two- and three-dimensional unsteady Euler equations using quadrilateral and hexhedral meshes, J. Comput. Phys., 175 (2002), 168–199.
[36] J. Zhou, L. Cai, J. -H. Feng and W. -X. Xie, Numerical simulation for two-phase flows using hybrid scheme, Appl. Math. comput., 186 (2007), 980–991.